Materials Today Chemistry 37 (2024) 102021

Contents lists available at ScienceDirect

Materials Today Chemistry

journal homepage: www.journals.elsevier.com/materials-today-chemistry/

'One-pot' engineering of 0D carbon-based inorganic nanoarchitectonics for boosting multitasking catalytic activity

Heting Hou [a], Jose Muñoz [a,*], I. Jénnifer Gómez [b], Nuria Romero [a], Xavier Sala [a], Jordi García-Antón [a,**]

[a] Departament de Química, Universitat Autònoma de Barcelona, 08193, Cerdanyola del Vallès, (Barcelona), Spain
[b] Centro Interdisciplinar de Química e Bioloxía (CICA), Universidade da Coruña, Rúa As Carballeiras, 15071 A Coruña, Spain

ARTICLE INFO

Keywords:
Sonocatalysis
Photocatalysis
Carbon dots
Metal nanoparticles
Hydrogen evolution reaction

ABSTRACT

Easy-to-make nanostructured materials that exhibit multitasking activity —while reducing the use of hazardous solvents throughout its architectural design— is a must to advance in the so-called Industry 4.0. Herein, a simple and eco-friendly 'one-pot' functionalization approach has been devised for synthesizing 0D carbon-based inorganic nanoarchitectonics made of carbon dots (CDs, as core carbon source) carrying two different inorganic building blocks, *viz.* quantum dots (CdSe@ZnS–QDs) and metal nanoparticles (Pt–NPs). As a proof-of-principle, the multi-catalytic activity of the resulting 0D Pt/QD/CD nanoarchitectonics by means of photoelectrocatalysis and sonocatalysis has been considered and compared with the pristine CD counterpart, demonstrating its suitability for boosting pivotal catalytic tasks like *i)* the photoelectrogeneration of hydrogen *via* hydrogen evolution reaction (HER), and *ii)* the sonodegradation of environmental pollutants (*i.e.*, Rhodamine B) in water. Overall, this chemical approach is general and might be tailored for architecting alternative carbon-based heterostructures to enhance alternative multi-catalytic tasks.

1. Introduction

Carbon nanomaterials, including 0D carbon dots (CDs), 1D carbon nanotubes, 2D graphene and 3D graphite, result very attractive from a Materials Chemistry point of view owing to their low cost, high stability, large-scale production, and tailorable surfaces [1–3]. Those characteristics along their outstanding and diverse physicochemical properties, make them play a key role in the so-called Industry 4.0 —also known as "Fourth Industrial Revolution"— by providing added value materials and devices easily integrable with current technologies [4,5].

In particular, CDs are a type of 0D carbon nanoallotrope predominantly composed of graphitic carbon (sp^2-hybridized carbon atoms), whose size is typically lower than 10 nm [6]. Since its discovery in 2004, CDs have been widely employed in a broad-spectrum of optical, electronic, catalytic and biological applications by taking advantage of their prominent physicochemical features, highlighting its inherent fluorescence activity, large surface area, and water solubility [7,8]. The ever-growing popularity of CDs is also substantiated by its rapid and straightforward preparation from cost-effective raw materials (including natural renewable sources). Amongst the different synthetic methods for CDs formation, the microwave-assisted hydrothermal tool is a powerful strategy for controlling the production of CDs with surface-engineered motifs [9–11]. This method relies on reacting small organic molecules (*e.g.*, glucose) with molecular components as doping (*viz.* R–X) under controlled hydrothermal conditions. (*i.e.*, temperature and pressure). Thus, part of the reactive X groups (*e.g.,* X: N, O, S) end up exposed on the CD surface, therefore promoting tunability for specific applications [12–18].

Architecting carbon-based heterostructures with different inorganic components has resulted in an effective path to provide nanoarchitectonics exhibiting multifunctional attributes, making it possible to obtain advanced materials with enhanced physicochemical features in general [19,20], and catalytic activity in particular [21–24]. To date, CDs have been functionalized with different inorganic building blocks –including quantum dots (QDs) and metal nanoparticles (MNPs)– to synthesize efficient catalysts made of 0D carbon-based inorganic nanoarchitectonics [25–30]. For example, while CDs carrying MNPs (*e.g.*, Pt–NPs) have shown to electrochemically catalyze the hydrogen

* Corresponding author
** Corresponding author.
E-mail addresses: josemaria.munoz@uab.cat (J. Muñoz), jordi.garciaanton@uab.cat (J. García-Antón).

https://doi.org/10.1016/j.mtchem.2024.102021
Received 27 November 2023; Received in revised form 29 February 2024; Accepted 18 March 2024
Available online 27 March 2024

evolution reaction (HER) *via* water splitting [31–34], CDs modified with QDs (*e.g.*, CdS–QDs) have displayed a catalytic effect for the sonodegradation of different dyes like Rhodamine B (RhB) [35,36]. Although efficient, the resulting 0D carbon-based inorganic nanoarchitectonics are only prepared to perform just a specific catalytic task [37–39].

Herein, a simple 'one-pot' synthetic approach has been devised in aqueous medium for engineering value-added 0D carbon-based inorganic nanoarchitectonics —made of CDs carrying two different inorganic moieties (*i.e.*, CdSe@ZnS–QDs and Pt–NPs)— for the development of functional nanomaterials capable of performing multitasking catalytic activity (see Scheme 1 for illustration). For this goal, CDs doped with both amino (–NH_2) and thiol (–SH) groups have been synthesized by simply reacting glucose with cysteamine (NH_2-CH_2-CH_2-SH) through a microwave-assisted hydrothermal method [19], resulting in surface-engineered motif N,S–CDs (Scheme 1A). Afterwards, 0D carbon-based inorganic nanoarchitectonics have been produced in aqueous medium *via* 'one-pot' reaction by functionalizing N,S–CDs with both CdSe@ZnS–QDs and Pt–NPs. While the terminal –SH groups are used for anchoring CdSe@ZnS–QDs *via* S–S bond formation [40], the terminal –NH_2 groups have been employed as supporting units to stabilize the *in situ* nucleation of Pt–NPs (Scheme 1B) [41]. Having verified the successful synthesis of the 0D Pt/QD/QD nanoarchitectonics through different characterization techniques, the multitasking catalytic activity has been demonstrated for boosting, as a proof-of-principle, *i)* the photoelectrogeneration of H_2 *via* HER and *ii)* the sonodegradation of an environmental pollutant as RhB. Scheme 1C summarizes the different catalytic approaches. In light with the state-of-the-art, this work provides a simple, rapid, and eco-friendly methodology for functionalizing CDs with several inorganic building blocks to provide value-added 0D carbon-based inorganic nanoarchitectonics exhibiting multitasking catalytic activity on-demand.

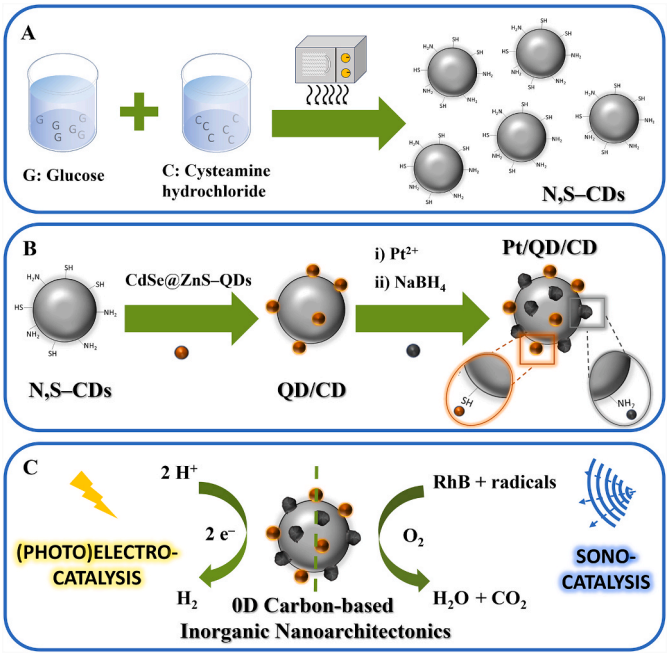

Scheme 1. Schematic illustration of the 'one-pot' synthesis and multicatalytic applications of 0D carbon-based inorganic nanoarchitectonics. **A)** Synthesis of pristine N,S–CDs *via* microwave-assisted hydrothermal method. **B)** Two-sequential steps for the engineering of 0D Pt/QD/CD nanoarchitectonics. **C)** Multitasking catalytic activity of 0D Pt/QD/CD nanoarchitectonics for the (photo)electocatalytic production of H_2 in acidic medium (left) and the sonocatalytic degradation of the RhB pollutant dye (right).

2. Experimental section

2.1. Chemicals and reagents

All of reagents are analytical grade and used without further purification. N,S–CDs precursors (glucose and cysteamine hydrochloride), Pt–NPs precursors ($[Pt(NH_3)_4](NO_3)_2$ and $NaBH_4$), CdSe@ZnS core-shell type quantum dots (CdSe@ZnS–QDs), Rhodamine B, and H_2SO_4 (98%) were purchased from Sigma-Aldrich. All solutions were prepared using Milli Q water (18.2 MΩ cm) from a Milli-Q system (Millipore, Billerica, MA, USA).

2.2. Synthesis of N,S–CDs

CDs rich in both –NH_2 and –SH groups (N,S–CDs) were synthesized by following our previous methodology [19]. Briefly, 5 mL of a 110 mM aqueous solution of glucose was mixed with 0.87 mmol of cysteamine hydrochloride. Then, the solution was placed in a microwave reactor (Discover SP microwave (CEM)) and heated at 250 W for 180 s. Afterwards, the sample was filtrated in order to remove the excess of unreacted reagents. Finally, the resulting N,S–CDs were obtained by dialyzing with molecular weight cut-off of 0.5–1 kDa against pure water for 48 h. The morphological aspect of the resulting N,S–CDs is depicted in Fig. S1, displaying typical quasispherical shapes.

2.3. 'One-pot' synthesis of 0D carbon-based inorganic nanoarchitectonics

The 'one-pot' synthesis of 0D carbon-based inorganic nanoarchitectonics made of Pt/QD/CD was carried out by two sequential steps under stirring conditions (see Scheme 1B). A 25 mL vial filled with 5 mL of an aqueous solution of N,S–CDs (3 mg mL^{-1}) was: *i)* firstly mixed with 50 μL of CdSe@ZnS core-shell QDs (1 mg mL^{-1}) for 12 h in order to promote the S–S chemical bond, and *ii)* subsequently loaded with 5 mL of 5.0 mM Pt^{2+} precursor ($[Pt(NH_3)_4](NO_3)_2$) for 2 h to preconcentrate the Pt^{2+} on N,S–CDs' surface, followed by the addition of a 10 mL of 0.1 M $NaBH_4$ to induce the nucleation and growth of Pt–NPs (a synthetic methodology known as IMS technique) [42–44]. Finally, the resulting 0D carbon-based inorganic nanoarchitectonics were centrifuged, washed thrice and dispersed with MilliQ water to obtain an stock solution of 1 mg mL^{-1}. For comparison, hybrids of QD/CD and Pt/CD were synthesized by mixing the N,S–CD precursor with either CdSe@ZnS core-shell QDs or Pt^{2+} precursor, respectively.

2.4. Characterization techniques

Material characterization of 0D carbon-based inorganic nanoarchitectonics was carried out by means of TEM (JEM-2011 unit with an acceleration voltage of 120 kV) and energy dispersive X-ray spectroscopy (EDS).

Electrocatalytic experiments were performed using an Origalys potentiostat, while the EC-Lab software was utilized for data acquisition. Experiments were run at room temperature in a three-electrode configuration cell filled with 1.0 M H_2SO_4 solution (pH 0), using Ag/AgCl (KCl sat.), a Pt wire, and glassy carbon (GC, Ø: 0.3 cm, A: 0.07 cm^2) as reference, counter and working electrodes, respectively. 15 μL of a fixed concentration of each material was drop-casted on the GC surface and dried at room temperature with air flow. Then, HER studies were recorded by lineal sweep voltammetry (LSV) with a scan rate of 5 mV s^{-1}, and the potential values (*vs.* Ag/AgCl) were converted to the standard RHE. For photoelectrocatalytic experiments, the aforementioned electrochemical setup was illuminated with a solar simulator (Xenon lamp, L.O.T. Oriel QuantumDesign, with a 395 nm filter). The distance from the solar simulator to the electrochemical cell was measured around 1 sun (100 mW cm^{-2}).

The sonocatalytic experiments for RhB degradation were carried out with an ultrasonic homogenizer (Cole Parmer 4710 series), operating at

an ultrasonic frequency of 90 KHz and output power of 75 W. During the experimental process, the output control tip (Ultrasonic Processor, Sonics, Vibra Cell, VCX 750, USA) was submerged in a 10 mL vial containing 0.025 mg mL^{-1} of RhB and 0.075 mg mL^{-1} of the studied materials. The reaction vial was placed in an ice bath to avoid overheating. Before ultrasonication, the solution was stirred for 30 min to ensure the establishment of an adsorption/desorption equilibrium of the dye on the sample surfaces. Finally, the sonocatalytic degradation of RhB was monitored during time by following the absorbance band decrease of RhB at $\lambda = 557$ nm *via* UV–vis spectroscopy (Agilent Cary 60 UV–Vis). The sonocatalytic degradation of RhB was considered as a pseudo-first-order reaction, and its kinetics was expressed following the formula:

$$ln\frac{C_0}{C_t} = kt$$

where k is the degradation rate constant and C_0 and C_t correspond to the RhB concentration (in mg·mL^{-1}) before and after any time t during ultrasonic irradiation, respectively.

3. Results and discussion

3.1. Characterization of 0D carbon-based inorganic nanoarchitectonics

Following the 'one-pot' synthetic procedure detailed above, the successful fabrication of 0D Pt/QD/CD nanoarchitectonics was confirmed by TEM coupled to EDX, as depicted in Fig. 1. For comparison, the TEM images of pristine N,S–CDs (blank sample), QD/CD and Pt/CD analogues (control samples) were also obtained.

Fig. 1A shows the morphological aspect of pristine N,S–CDs displaying a typical carbonaceous dark surface. Considering the expected high contrast from CdSe@ZnS–QDs and Pt–NPs over the CDs, a high concentration sample (3 mg mL^{-1}) was utilized, resulting in agglomerated systems [19]. After material functionalization, spherical nanoparticles dispersed throughout the whole carbonaceous material were observed on the surface of the 0D Pt/QD/CD nanoarchitectonics (Fig. 1B), suggesting the successful integration of both CdSe@ZnS–QDs and Pt–NPs. Importantly, two different types of nanoparticles can be clearly identified: *i)* darker and bigger nanoparticles with an average size of 14.8 ± 6.9 nm, which fits well with the ones observed at the Pt/CD control (Fig. 1C), and *ii)* smaller and lightly-colored nanoparticles with a mean size diameter of 3.3 ± 1.3 nm, which are in line with the morphology displayed at the QD/CD control (Fig. 1D). Further, EDX analyses were conducted to verify the presence of CdSe@ZnS–QDs and Pt–NPs in the 0D Pt/QD/CD nanoarchitectonic. The EDX spectrum of pristine N,S–CDs (Fig. 1E) displayed C, O, N and S as main elements, whereas the EDX spectrum of 0D Pt/QD/CD nanoarchitectonics (Fig. 1F) evidenced the additional presence of Zn (from the shell of QDs) and Pt. Consequently, it is safe to conclude that both CdSe@ZnS–QDs and Pt–NPs were anchored on the surface of N,S–CDs.

3.2. Multicatalytic performance of 0D carbon-based inorganic nanoarchitectonics

Having verified the successful synthesis of 0D carbon-based inorganic nanoarchitectonics, the multitask catalytic activity was explored in two important fields: energy conversion and water remediation.

Photoelectrocatalytic production of H_2 via HER: On the one hand, the feasibility of exploring 0D carbon-based inorganic nanoarchitectonics as unconventional photoelectrocatalysts in the energy conversion field was tested by means of HER. Briefly, molecular hydrogen (H_2) has been positioned as an ideal renewable energy source owing to its high gravimetric energy density and the environmental benignity when used as a fuel, just producing water during combustion [45–47]. In this line, HER is known to be the simplest (photo)electrocatalytic reaction, which relates the reduction of protons (H^+) to H_2 *via* a two-electron transfer process [47,48].

Fig. 2 shows the linear sweep voltammograms performed in 1 M H_2SO_4 in presence and absence of solar light irradiation, and the HER performance was compared to other catalytic systems using the overpotential achieved at a standard current density value (−10 mA cm^{-2}). For this goal, 3 measurements ($n = 3$) were performed in order to observe the reproducibility of the system. Fig. 2A depicts the HER performance of pristine N,S–CDs, which exhibited a poor (photo)electrocatalytic activity for HER with overpotentials as high as 652 mV (in

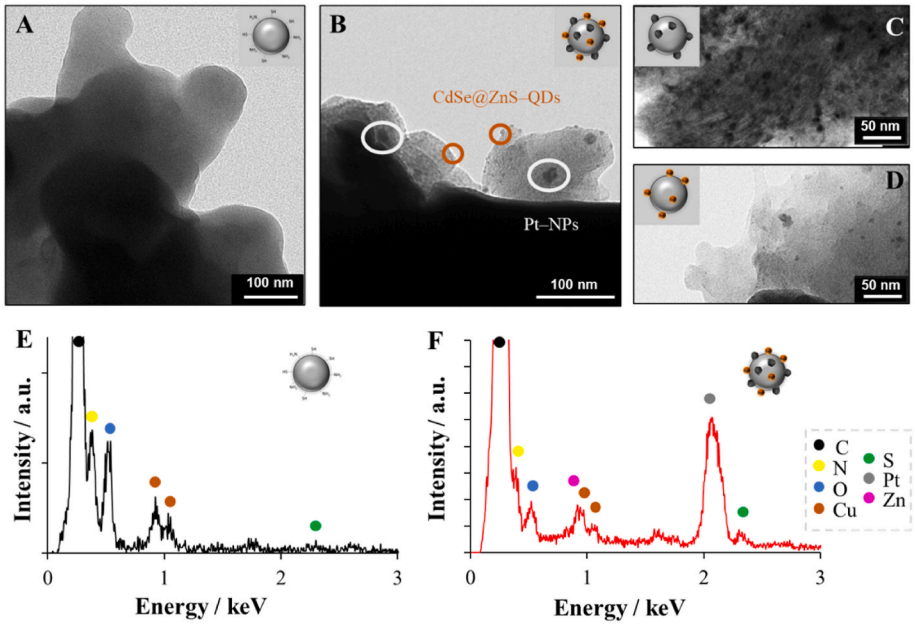

Fig. 1. Material characterization of 0D carbon-based inorganic nanoarchitectonics. A) TEM images of pristine N,S–CDs, **B)** 0D Pt/QD/CD nanoarchitectonics –highlighting CdSe@ZnS–QDs (orange) and Pt–NPs (grey)–, and control materials: **C)** Pt/CD and **D)** QD/CD. EDX elemental analysis of **E)** pristine N,S–CDs and **F)** 0D Pt/QD/CD nanoarchitectonics. Note: the Cu content provides from the grill used for the measurements. (For interpretation of the references to color in this figure legend, the reader is referred to the Web version of this article.)

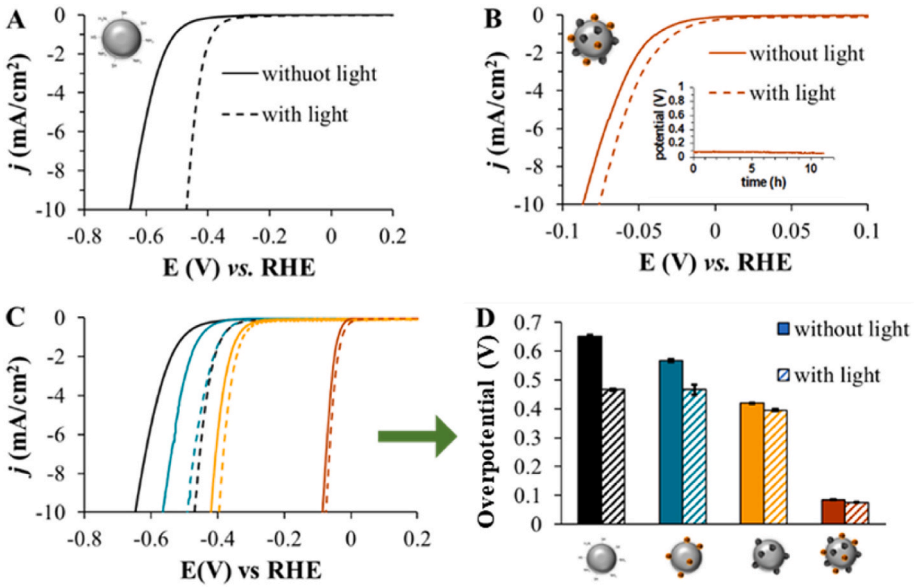

Fig. 2. Photoelectrocatalytic HER performance of 0D carbon-based inorganic nanoarchitectonics. Polarization curves of **A)** pristine N,S–CDs and **B)** 0D Pt/QD/CD nanoarchitectonics in absence (solid line) and presence of solar light irradiation (dashed line). Inset: short-term stability test at −10 mA·cm^{-2} current density. **C)** Comparison of the polarization curves obtained using pristine N,S–CDs (black), QD/CD (green), Pt/CD (orange) and 0D Pt/QD/CD nanoarchitectonics (red) in presence (solid line) and absence (dashed line) of solar light irradiation with **D)** their corresponding overpotential summary, also displaying the error bars from the three different measurements (n = 3). LSV experiments were carried out in a 1.0 M H_2SO_4 electrolyte solution at scan rate of 5 mV·s^{-1}. (For interpretation of the references to color in this figure legend, the reader is referred to the Web version of this article.)

absence of solar light irradiation) and 466 mV (under illumination). The expected overpotential improvement after solar light irradiation is ascribed to the inherent semiconducting properties of CDs [1,8]. Importantly, such overpotential was significantly enhanced after functionalization with both CdSe@ZnS–QDs and Pt–NPs, yielding to values as low as 86 and 76 mV before and after solar light irradiation, respectively. This results in an overpotential improvement of more than 6 times. In addition, a stability test was conducted for 10 h, indicating that the 0D Pt/QD/CD nanoarchitectonics are stable in the mid-long term (Fig. 2B, inset). For comparison, additional HER analyses were carried out using CD/QD and CD/Pt counterparts as control experiments. As shown in Fig. 2C and D, the HER performance of pristine N,S–CDs was clearly improved after functionalization with either CdSe@ZnS–QDs or Pt–NPs, with overpotentials values of 568 mV and 466 mV for QD/CD and 419 mV and 396 mV for Pt/CD, in absence and presence of solar light irradiation, respectively. Nonetheless, those values are far from the ones achieved by the 0D Pt/QD/CD nanoarchitectonics, demonstrating the synergistic effect of combining two inorganic nanoparticles in a same carbonaceous nanotemplate. Such synergia can be ascribed to *i)* the well-known catalytic effect of Pt–NPs owing to the close-to-optimal interaction with adsorbed hydrogen (H*) atoms —considered as one of the main descriptors for the HER activity according to Sabatier's principle [49], in combination with *ii)* the capability of QDs to facilitate the general electron transfer rates of the system [50], fact that can favor the electron transfer process for the concomitant reduction of H^+ to H_2 on the resulting 0D Pt/QD/CD nanoarchitectonics [51].

Comparing to the state-of-the-art CD-based materials for HER performance, the overpotential yielded by the developed 0D carbon-based inorganic nanoarchitectonics in acidic medium (76 mV under solar light irradiation) is one of the lowest found in literature (see Table S1), demonstrating to be a promising photocatalyst for energy conversion applications.

Then, the reaction kinetics of the different materials were evaluated by means of Tafel plots, using the polarization curves from Fig. 2C. As shown in Fig. S2, the experimentally-determined Tafel slope values decreased as follows: pristine N,S–CD > QD/CD > Pt/CD > Pt/QD/CD, while a favorable HER kinetics was observed under solar light irradiation. The Tafel slope value of 79 mV·dec^{-1} (dark) and 71 mV·dec^{-1} (light irradiation) yielded by the 0D carbon-based inorganic nanoarchitectonic determines a Volmer-Heyrovsky mechanism for HER [52]. Further, the electrochemically active surface area (ECSA) of pristine N,S–CDs and 0D Pt/QD/CD nanoarchitectonics was estimated from the double layer capacitance (C_{dl}) value obtained by CV within a non-Faradaic region at different scan rates (Fig. S3). As a result, the ECSA for 0D Pt/QD/CD nanoarchitectonics (1.0 cm^2) was larger than that of pristine N,S–CDs (0.2 cm^2), demonstrating its enhanced electrochemical activity. Finally, these results are also consistent with the Nyquist plots of the electrochemical impedance spectroscopy (EIS) measurements (Fig. S4). Remarkably, the 0D carbon-based inorganic nanoarchitectonics displayed a lower semi-circle when compared with the pristine N,S–CD counterpart (95.3 *vs.* 317.2 Ω). Since the R_{CT} parameter is inversely proportional to the current density, it can be concluded that 0D Pt/QD/CD nanoarchitectonics exhibit a more efficient electron transfer, and thus higher HER activity [53].

Based on the results above, a possible photocatalytic mechanism of 0D carbon-based inorganic nanoarchitectonics is proposed in Fig. S5. Upon solar light irradiation, photoinduced charge separation (electrons, e^- and holes, h^+) can occur in N,S–CDs owing to the absorbance band in the visible range (420 nm, see Fig. S6), resulting in an estimated band gap of 2.94 eV. Then, the N,S–CDs can serve as electron donor, promoting the migration of these electrons to the conduction band of CdSe@ZnS–QDs, which must be immediately transferred to the Pt–NPs to promote the reduction of protons (H^+) to hydrogen gas (H_2) [54]. Meanwhile, the photo-generated h^+ left in the valence band of N,S–CDs results in the oxidation of water (H_2O) to oxygen gas (O_2).

Sonocatalytic degradation of RhB: On the other hand, the applicability of 0D carbon-based inorganic nanoarchitectonics in the field of water remediation was also interrogated by exploring the sonocatalytic degradation of pollutant dyes, using RhB as a model target. The treatment of organic dye wastewater is an urgent environmental challenge owing to their toxic effects on the ecological environment [55,56]. In the last decade, sonocatalytic degradation process has become an interesting way to degrade organic dyes *via* a chemical effect of ultrasonic

waves (US) that promotes the formation of highly reactive radical species (*e.g.,* •OH, •H, •O and $O_2^{\bullet-}$) capable of completely oxidize organic pollutants into CO_2 and H_2O [57–59].

The sonocatalytic activity of 0D carbon-based inorganic nanoarchitectonics towards the degradation of RhB was explored by monitoring the absorbance band of RhB *via* UV–vis spectroscopy (Fig. 3). For this aim, 0.025 mg mL^{-1} of RhB were mixed with 0.075 mg mL^{-1} of 0D Pt/QD/CD nanoarchitectonics. After preconcentrating for 30 min under stirring conditions, the sample was sonicated at 75 W and optically monitored at different US exposure times. As shown in Fig. 3A, the inherent absorbance band of RhB at $\lambda = 557$ nm decreases with increasing the ultrasonic time. As shown in Fig. 3B, after 150 min ultrasonic exposure, RhB was almost completely degraded, presenting a sonocatalytic capacity (C/C_0) of 0.038, where C_0 and C correspond to the concentration of RhB before and after each ultrasonic time, respectively. The Langmuir–Hinshelwood model was applied to calculate the pseudo-first-order reaction constant (*k*), yielding to a value of 0.021 min^{-1} (Fig. 3B, inset). In addition, the stability and reusability of the 0D carbon-based inorganic nanorachitectonics was also explored by carrying out three different degradation cycles. For this goal, the 0D Pt/QD/CD nanoarchitectonics were centrifuged after each cycle and reused with a fresh RhB solution. The sonocatalytic graphs shown in Fig. 3C clearly indicate that the 0D carbon-based inorganic nanoarchitectonics were highly stable for three consecutive cycles, since no significant changes in the degradation activity can be noticed. As shown in TEM image of Fig. S7, no evidence of nanoparticles leakage was observed after the sonocatalytic degradation of RhB, demonstrating the stability of the 0D carbon-based inorganic nanoarchitectonics.

Subsequently, the sonocatalytic activity of 0D Pt/QD/CD nanoarchitectonics was compared to the one exhibited by pristine N,S–CDs (blank experiment) at a fixed ultrasonic time (30 min). As depicted in Fig. 3D, while the sonocatalytic activity of 0D Pt/QD/CD nanoarchitectonics was 52% after 30 min ultrasonic exposure, N,S–CDs presented a lower sonocatalytic activity of 19%. This indicates that the sonocatalytic activity of 0D Pt/QD/CD nanoarchitectonics is improved by 63.5%. In addition, control experiments with QD/CD and Pt/CD also revealed lower sonocatalytic activity when compared to 0D carbon-based inorganic nanoarchitectonics, yielding to values of 40% and 35%, respectively. Consequently, the synergistic effect of combining both CdSe@ZnS–QDs and Pt–NPs in a same carbonaceous nanomaterial also allows the development of sonocatalysts with enhanced catalytic activity.

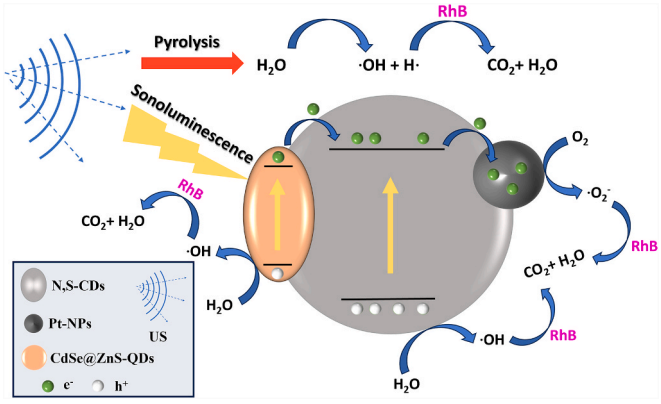

Fig. 4. Proposed sonocatalytic mechanism for the degradation of RhB using 0D carbon-based inorganic nanoarchitectonics. While a pyrolytic effect is the main responsible for RhB degradation using pristine N,S–QDs, the generated sonoluminescence can favor the generation of further radical species when both CdSe@ZnS–QDs and Pt–NPs are present in the system, fact that assists the degradation process.

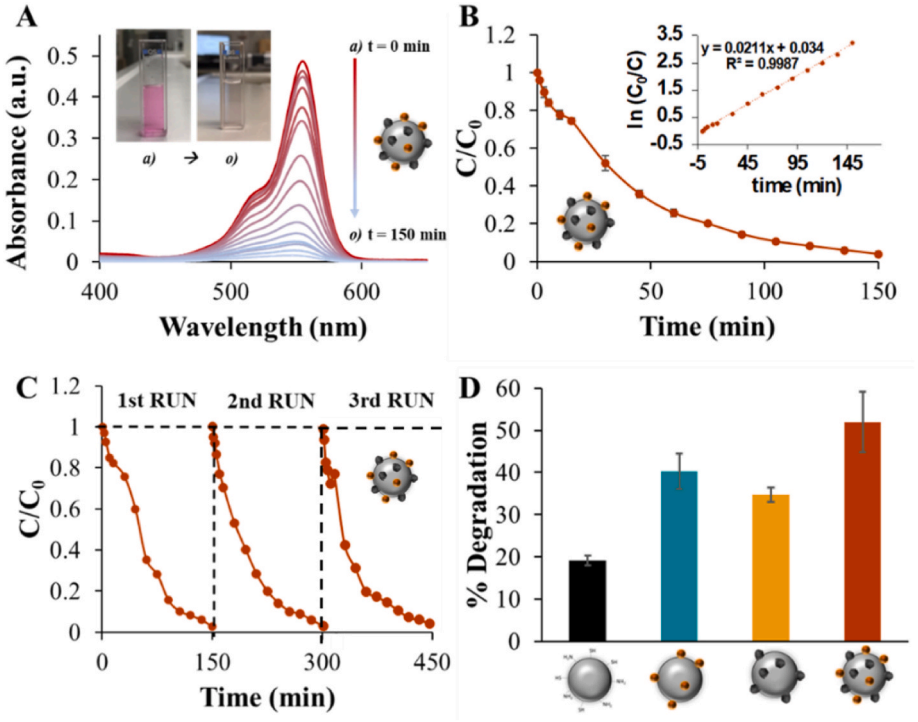

Fig. 3. Sonocatalytic performance of 0D carbon-based inorganic nanoarchitectonics towards RhB degradation. A) Absorption changes of 0.025 mg mL^{-1} RhB in presence of 0.075 mg mL^{-1} of 0D Pt/QD/CD nanoarchitectonics, with its corresponding **B)** degradation evolution curve after various ultrasonic times (inset: kinetic study of catalytic degradation) and **C)** repeatability test during three consecutive sonocatalytic experiments. **D)** Control experiments displaying the sonocatalytic activity of pristine N,S–CDs (black), QD/CD (blue), Pt/CD (orange) towards the degradation of RhB at a fixed ultrasonic time (t = 30 min), and comparison with regarding the results obtained by 0D Pt/QD/CD nanoarchitectonics (red). (For interpretation of the references to color in this figure legend, the reader is referred to the Web version of this article.)

Finally, Fig. 4 illustrates the proposed synergistic sonocatalytic mechanism for boosting RhB degradation. Under ultrasound power, cavitation micro-vapor bubbles are initially formed and quickly collapse, emitting a burst of light —phenomenon known as sonoluminiscence— that promotes a pyrolytic process that induces the formation of highly active radical species like •OH and •H, (Eq. (1)) [60–64]. This bust of light can excite electrons from the valence band of CDs to the conductive band, yielding to electron–hole (e^-–h^+) pairs (Eq. (2)). Then, this e^-–h^+ pairs can further form $O_2^{\bullet-}$ (Eq. (3)) and •OH (Eq. (4)), which can be utilized to degrade RhB to CO_2 and H_2O (Eq. (5)).

$$H_2O + Ultrasounds \rightarrow \bullet OH + \bullet H \quad \text{Eq. 1}$$

$$CD + Ultrasounds \rightarrow e^- + h^+ \quad \text{Eq. 2}$$

$$e^- + O_2 \rightarrow O_2\cdot- \quad \text{Eq. 3}$$

$$h^+ + H_2O \rightarrow \bullet OH \quad \text{Eq. 4}$$

$$RhB + Sonocatalyst + \bullet OH + O_2\cdot- + Ultrasounds \rightarrow H_2O + CO_2 \quad \text{Eq. 5}$$

However, when both CdSe@ZnS–QDs and Pt–NPs are also present in the system, it is expected that such sonoluminescence phenomenon also induces the excitation of e^- from the valence band of QDs, which should be transferred to the conductive band of CDs. Simultaneously, the h^+ generated at CDs and QDs will lead the formation of •OH. Further, the presence of metallic centres like Pt–NPs can contribute to greatly enhance the generation of reactive radical species for the fast degradation of RhB [65]. All in all, the integration of both inorganic nanoparticles in the carbonaceous system promotes a faster separation of e^-–h^+ pairs while increases the concentration of radical species in the medium, leading to a faster degradation process.

4. Conclusions

Overall, 0D carbon-based inorganic nanoarchitectonics made of N, S–CDs, CdSe@ZnS–QDs and Pt–NPs were successfully synthesized *via* 'one-pot' method in aqueous medium. As a first proof-of-principle, the multitasking catalytic activity of the resulting 0D Pt/QD/CD nanoarchitectonics was tested in two different processes, such as *i)* the photoelectrogeneration of H_2 *via* HER, and *ii)* the sonocatalytic degradation of RhB. Interestingly, both catalytic tasks were significantly boosted once both inorganic nanoparticles were incorporated to the carbonaceous system. Comparing to the results obtained by the pristine N,S–CDs, the photoelectrochemical HER overpotential was improved by >6 times, while the sonodegradation activity of RhB was enhanced by 63.5%. Consequently, this proof-of-concept demonstrates the suitability of combining multiple inorganic building blocks in a same carbonaceous surface for the development of value-added nanocatalysts exhibiting excellent multitasking activity. Finally, this method is general and could be extended by tailoring either the carbonaceous core material or the inorganic building blocks.

CRediT authorship contribution statement

Heting Hou: Writing – original draft, Investigation, Formal analysis, Data curation. **Jose Muñoz:** Writing – review & editing, Writing – original draft, Validation, Supervision, Data curation, Conceptualization. **I. Jénnifer Gómez:** Writing – review & editing, Investigation. **Nuria Romero:** Writing – review & editing, Supervision. **Xavier Sala:** Writing – review & editing, Validation, Resources, Funding acquisition. **Jordi García-Antón:** Writing – review & editing, Supervision, Funding acquisition.

Declaration of competing interest

The authors declare that they have no known competing financial interests or personal relationships that could have appeared to influence the work reported in this paper.

Data availability

Data will be made available on request.

Acknowledgments

H. H. acknowledges the program of China Scholarships Council (No. 201908440337). X.S. thanks ICREA for the ICREA Academia Prize 2020. X.S. and J.G.-A. thank MINECO/FEDER for financial support (PID2019-104171RB-I00). J. M. is indebted to the Ramón y Cajal Program (RYC2021-033820-I Fellowship) funded by MCIN/AEI/10.13039/501100011033 and by the European Union "NextGenerationEU/PRTR". I. J. G. acknowledges the Spanish Ministry of Universities for a Beatriz Galindo (BG22/000147) and Maria Zambrano funding (RSU.UDC. MZ09) transferred by the European Union-Next GenerationEU.

Appendix A. Supplementary data

Supplementary data to this article can be found online at https://doi.org/10.1016/j.mtchem.2024.102021.

References

[1] H. Yu, R. Shi, Y. Zhao, G.I.N. Waterhouse, L.Z. Wu, C.H. Tung, T. Zhang, Smart utilization of carbon dots in semiconductor photocatalysis, Adv. Mater. 28 (2016) 9454–9477, https://doi.org/10.1002/adma.201602581.
[2] C. Xia, S. Zhu, T. Feng, M. Yang, B. Yang, Evolution and synthesis of carbon dots: from carbon dots to carbonized polymer dots, Adv. Sci. 6 (2019), https://doi.org/10.1002/advs.201901316.
[3] S. Goriparti, E. Miele, F. De Angelis, E. Di Fabrizio, R. Proietti Zaccaria, C. Capiglia, Review on recent progress of nanostructured anode materials for Li-ion batteries, J. Power Sources 257 (2014) 421–443, https://doi.org/10.1016/j.jpowsour.2013.11.103.
[4] P. Mayorga-Burrezo, J. Muñoz, D. Zaoralová, M. Otyepka, M. Pumera, Multiresponsive 2D Ti3C2TxMXene via implanting molecular properties, ACS Nano 15 (2021) 10067–10075, https://doi.org/10.1021/acsnano.1c01742.
[5] M. Notarianni, J. Liu, K. Vernon, N. Motta, Synthesis and applications of carbon nanomaterials for energy generation and storage, Beilstein J. Nanotechnol. 7 (2016) 149–196, https://doi.org/10.3762/bjnano.7.17.
[6] S.N. Baker, G.A. Baker, Luminescent carbon nanodots: emergent nanolights, Angew. Chem. Int. Ed. 49 (2010) 6726–6744, https://doi.org/10.1002/anie.200906623.
[7] X. Xu, R. Ray, Y. Gu, H.J. Ploehn, L. Gearheart, K. Raker, W.A. Scrivens, Electrophoretic analysis and purification of fluorescent single-walled carbon nanotube fragments, J. Am. Chem. Soc. 126 (2004) 12736–12737, https://doi.org/10.1021/ja040082h.
[8] A.M. El-Shafey, Carbon dots: discovery, structure, fluorescent properties, and applications, Green Process. Synth. 10 (2021) 134–156, https://doi.org/10.1515/gps-2021-0006.
[9] T.T. Hoang, H.P. Pham, Q.T. Tran, A facile microwave-assisted hydrothermal synthesis of graphene quantum dots for organic solar cell efficiency improvement, J. Nanomater. 2020 (2020) 15–17, https://doi.org/10.1155/2020/3207909.
[10] I.J. Gómez, M. Vázquez Sulleiro, A. Dolečková, N. Pizúrová, J. Medalová, R. Roy, D. Nečas, L. Zajíčková, Exploring the emission pathways in nitrogen-doped graphene quantum dots for bioimaging, J. Phys. Chem. C 125 (2021) 21044–21054, https://doi.org/10.1021/acs.jpcc.1c06029.
[11] I.J. Gómez, M.V. Sulleiro, A. Dolečková, N. Pizúrová, J. Medalová, A. Bednařík, J. Preisler, D. Nečas, L. Zajíčková, Structure elucidation of multicolor emissive graphene quantum dots towards cell guidance, Mater. Chem. Front. 6 (2022) 145–154, https://doi.org/10.1039/d1qm01126j.
[12] S. Ren, M. Cui, X. Chen, S. Mei, Y. Qiang, Comparative study on corrosion inhibition of N doped and N,S codoped carbon dots for carbon steel in strong acidic solution, J. Colloid Interface Sci. 628 (2022) 384–397, https://doi.org/10.1016/j.jcis.2022.08.070.
[13] T.V. De Medeiros, J. Manioudakis, F. Noun, J.R. Macairan, F. Victoria, R. Naccache, Microwave-assisted synthesis of carbon dots and their applications, J. Mater. Chem. C 7 (2019) 7175–7195, https://doi.org/10.1039/c9tc01640f.
[14] F. Nemati, M. Hosseini, R. Zare-Dorabei, F. Salehnia, M.R. Ganjali, Fluorescent turn on sensing of Caffeine in food sample based on sulfur-doped carbon quantum dots and optimization of process parameters through response surface methodology, Sens. Actuators, B 273 (2018) 25–34, https://doi.org/10.1016/j.snb.2018.05.163.
[15] S. Konar, B.N.P. Kumar, M.K. Mahto, D. Samanta, M.A.S. Shaik, M. Shaw, M. Mandal, A. Pathak, N-doped carbon dot as fluorescent probe for detection of cysteamine and multicolor cell imaging, Sens. Actuators, B 286 (2019) 77–85, https://doi.org/10.1016/j.snb.2019.01.117.

[16] F. Liao, Y. Shi, Q. Dang, H. Yang, H. Huang, Z. Kang, M. Shao, Carbon dots dominated photoelectric surface in titanium dioxide nanotube/nitrogen-doped carbon dot/gold nanocomposites for improved photoelectrochemical water splitting, J. Colloid Interface Sci. 606 (2022) 1274–1283, https://doi.org/10.1016/j.jcis.2021.08.131.

[17] I. J. Gómez, M. Russo, O.A. Arcidiacono, E.M. Sánchez-Carnerero, P. Klán, L. Zajíčková, Coupling BODIPY with nitrogen-doped graphene quantum dots to address the water solubility of photosensitizers, Mater. Chem. Front. 6 (2022) 1719–1726, https://doi.org/10.1039/d2qm00200k.

[18] Y. Huang, W. Zhou, W. Kong, L. Chen, X. Lu, H. Cai, Y. Yuan, L. Zhao, Y. Jiang, H. Li, L. Wang, L. Wang, H. Wang, J. Zhang, J. Gu, Z. Fan, Atomically interfacial engineering on molybdenum nitride quantum dots decorated N-doped graphene for high-rate and stable alkaline hydrogen production, Adv. Sci. 9 (2022) 1–12, https://doi.org/10.1002/advs.202204949.

[19] J. Muñoz, M. Palacios-Corella, I.J. Gómez, L. Zajíčková, M. Pumera, Synthetic nanoarchitectonics of functional organic–inorganic 2D germanane heterostructures via click Chemistry, Adv. Mater. 34 (2022) 1–8, https://doi.org/10.1002/adma.202206382.

[20] M. Vázquez Sulleiro, A. Develioglu, R. Quirós-Ovies, L. Martín-Pérez, N. Martín Sabanés, M.L. Gonzalez-Juarez, I.J. Gómez, M. Vera-Hidalgo, V. Sebastián, J. Santamaría, E. Burzurí, E.M. Pérez, Fabrication of devices featuring covalently linked MoS2–graphene heterostructures, Nat. Chem. 14 (2022) 695–700, https://doi.org/10.1038/s41557-022-00924-1.

[21] C.R. Kagan, D.B. Mitzi, C.D. Dimitrakopoulos, Organic-inorganic hybrid materials as semiconducting channels in thin- film field-effect transistors, Science 286 (1999) 945–947, https://doi.org/10.1126/science.286.5441.945.

[22] F. Liu, W.L. Chow, X. He, P. Hu, S. Zheng, X. Wang, J. Zhou, Q. Fu, W. Fu, P. Yu, Q. Zeng, H.J. Fan, B.K. Tay, C. Kloc, Z. Liu, Van der Waals p-n junction based on an organic-inorganic heterostructure, Adv. Funct. Mater. 25 (2015) 5865–5871, https://doi.org/10.1002/adfm.201502316.

[23] J. Muñoz, D. Rojas, M. Pumera, Faceted crystal nanoarchitectonics of organic-inorganic 3D-printed visible-light photocatalysts, ACS Appl. Energy Mater. 5 (2022) 3252–3258, https://doi.org/10.1021/acsaem.1c03863.

[24] J. Muñoz, E. Redondo, M. Pumera, Versatile design of functional organic–inorganic 3D-printed (Opto)Electronic interfaces with custom catalytic activity, Small 17 (2021) 1–9, https://doi.org/10.1002/smll.202103189.

[25] D. Dey, T. Bhattacharya, B. Majumdar, S. Mandani, B. Sharma, T.K. Sarma, Carbon dot reduced palladium nanoparticles as active catalysts for carbon-carbon bond formation, Dalton Trans. 42 (2013) 13821–13825, https://doi.org/10.1039/c3dt51234g.

[26] J. Muñoz, J. Bastos-Arrieta, M. Muñoz, D. Muraviev, F. Céspedes, M. Baeza, CdS quantum dots as a scattering nanomaterial of carbon nanotubes in polymeric nanocomposite sensors for microelectrode array behavior, J. Mater. Sci. 51 (2016) 1610–1619, https://doi.org/10.1007/s10853-015-9484-0.

[27] X. Li, B. Li, Q. Zhang, X. Li, Preparation of carbon dots-metal nanoparticles nanocomposites and their application in heterogeneous catalysis, Nano Futures 7 (2023) 42001, https://doi.org/10.1088/2399-1984/ad03b2.

[28] F. Li, Y. Liu, B. Mao, L. Li, H. Huang, D. Zhang, W. Dong, Z. Kang, W. Shi, Carbon-dots-mediated highly efficient hole transfer in I-III-VI quantum dots for photocatalytic hydrogen production, Appl. Catal. B Environ. 292 (2021) 120154, https://doi.org/10.1016/j.apcatb.2021.120154.

[29] Q. Hu, K. Liu, J. Ye, L. Ming, J. Xu, S. Cao, Hierarchical Pt/NiCo2O4 nanosheets decorated carbon nanofibers for room-temperature catalytic formaldehyde oxidation, Appl. Surf. Sci. 623 (2023) 157012, https://doi.org/10.1016/j.apsusc.2023.157012.

[30] F. Xu, K. Meng, S. Cao, C. Jiang, T. Chen, J. Xu, J. Yu, Step-by-Step mechanism insights into the TiO2/Ce2S3 S-scheme photocatalyst for enhanced aniline production with water as a proton source, ACS Catal. 12 (2022) 164–172, https://doi.org/10.1021/acscatal.1c04903.

[31] W. Chen, J. Shen, Y. Huang, X. Liu, D. Astruc, Catalyzed hydrolysis of tetrahydroxydiboron by graphene quantum dot-stabilized transition-metal nanoparticles for hydrogen evolution, ACS Sustain. Chem. Eng. 8 (2020) 7513–7522, https://doi.org/10.1021/acssuschemeng.0c02496.

[32] Q. Dang, Y. Sun, X. Wang, W. Zhu, Y. Chen, F. Liao, H. Huang, M. Shao, Carbon dots-Pt modified polyaniline nanosheet grown on carbon cloth as stable and high-efficient electrocatalyst for hydrogen evolution in pH-universal electrolyte, Appl. Catal. B Environ. 257 (2019) 117905, https://doi.org/10.1016/j.apcatb.2019.117905.

[33] B. Hu, K. Huang, B. Tang, Z. Lei, Z. Wang, H. Guo, C. Lian, Z. Liu, L. Wang, Graphene quantum dot-mediated atom-layer semiconductor electrocatalyst for hydrogen evolution, Nano-Micro Lett. 15 (2023) 1–15, https://doi.org/10.1007/s40820-023-01182-7.

[34] L. Chen, Y. Huang, Y. Ding, P. Yu, F. Huang, W. Zhou, L. Wang, Y. Jiang, H. Li, H. Cai, L. Wang, H. Wang, M. Liao, L. Zhao, Z. Fan, Interfacial Engineering of Atomic Platinum-Doped Molybdenum Carbide Quantum Dots for High-Rate and Stable Hydrogen Evolution Reaction in Proton Exchange Membrane Water Electrolysis, vol. 16, 2023, pp. 12186–12195.

[35] S. Sajjadi, A. Khataee, M. Kamali, Sonocatalytic degradation of methylene blue by a novel graphene quantum dots anchored CdSe nanocatalyst, Ultrason. Sonochem. 39 (2017) 676–685, https://doi.org/10.1016/j.ultsonch.2017.05.030.

[36] K.S. Sharma, A. Mudgal, M. Nair, D. Kumar, AND logic gate supported novel speckled phosphorus-doped carbon dots decorated ZrO2/CaO/MgO sonocatalysts for efficient MB dye decolorization, Mater. Chem. Phys. 290 (2022) 126609, https://doi.org/10.1016/j.matchemphys.2022.126609.

[37] A.P. Wight, M.E. Davis, Design and preparation of organic-inorganic hybrid catalysts, Chem. Rev. 102 (2002) 3589–3614, https://doi.org/10.1021/cr010334m.

[38] J. Azadmanjiri, J. Wang, C.C. Berndt, A. Yu, 2D layered organic-inorganic heterostructures for clean energy applications, J. Mater. Chem. A 6 (2018) 3824–3849, https://doi.org/10.1039/c8ta00132d.

[39] G. Sun, J. Zhang, B. Cheng, H. Yu, J. Yu, J. Xu, Bifunctional CdS/COF S-scheme photocatalyst for enhanced H2 evolution and organic synthesis, Chem. Eng. J. 476 (2023) 146818, https://doi.org/10.1016/j.cej.2023.146818.

[40] J. Muñoz, M. Urso, M. Pumera, Self-propelled multifunctional microrobots harboring chiral supramolecular selectors for “enantiorecogniton-on-the-fly,”, Angew. Chem. 134 (2022) 1–7, https://doi.org/10.1002/ange.202116090.

[41] S. Wang, Z. Ai, X. Niu, W. Yang, R. Kang, Z. Lin, A. Waseem, L. Jiao, H.L. Jiang, Linker engineering of sandwich-structured metal–organic framework composites for optimized photocatalytic H2 production, Adv. Mater. 2302512 (2023) 1–7, https://doi.org/10.1002/adma.202302512.

[42] J. Muñoz, E. Redondo, M. Pumera, Bistable (supra)molecular switches on 3D-printed responsive interfaces with electrical readout, ACS Appl. Mater. Interfaces. 13 (2021) 12649–12655, https://doi.org/10.1021/acsami.0c14487.

[43] J. Macanás, M. Farre, M. Muñoz, S. Alegret, D.N. Muraviev, Preparation and characterization of polymer-stabilized metal nanoparticles for sensor applications, Physica Status Solidi (A) Applications and Materials Science 203 (2006) 1194–1200, https://doi.org/10.1002/pssa.200566167.

[44] J. Bastos-Arrieta, J. Muñoz, A. Stenbock-Fermor, M. Muñoz, D.N. Muraviev, F. Céspedes, L.A. Tsarkova, M. Baeza, Intermatrix Synthesis as a rapid, inexpensive and reproducible methodology for the in situ functionalization of nanostructured surfaces with quantum dots, Appl. Surf. Sci. 368 (2016) 417–426, https://doi.org/10.1016/j.apsusc.2016.01.277.

[45] W. Zhang, Q. Xu, X. Tang, H. Jiang, J. Shi, V. Fominski, Y. Bai, P. Chen, J. Zou, Construction of a transition-metal sulfide heterojunction photocatalyst driven by a built-in electric field for efficient hydrogen evolution under visible light, J. Colloid Interface Sci. 649 (2023) 325–333, https://doi.org/10.1016/j.jcis.2023.06.080.

[46] M. Momirlan, T.N. Veziroglu, Current status of hydrogen energy, Renew. Sustain. Energy Rev. 6 (2002) 141–179, https://doi.org/10.1016/S1364-0321(02)00004-7.

[47] P. Kuang, M. Sayed, J. Fan, B. Cheng, J. Yu, 3D graphene-based H2-production photocatalyst and electrocatalyst, Adv. Energy Mater. 10 (2020) 1–53, https://doi.org/10.1002/aenm.201903802.

[48] Z. Wang, C. Li, K. Domen, Recent developments in heterogeneous photocatalysts for solar-driven overall water splitting, Chem. Soc. Rev. 48 (2019) 2109–2125, https://doi.org/10.1039/c8cs00542g.

[49] M. Smiljanić, S. Panić, M. Bele, F. Ruiz-Zepeda, L. Pavko, L. Gašparič, A. Kokalj, M. Gaberščček, N. Hodnik, Improving the HER activity and stability of Pt nanoparticles by titanium oxynitride support, ACS Catal. 12 (2022) 13021–13033, https://doi.org/10.1021/acscatal.2c03214.

[50] C. Xue, H. Li, H. An, B. Yang, J. Wei, G. Yang, NiSx quantum dots accelerate electron transfer in Cd0.8Zn0.2S photocatalytic system via an rGO nanosheet “bridge” toward visible-light-driven hydrogen evolution, ACS Catal. 8 (2018) 1532–1545, https://doi.org/10.1021/acscatal.7b04228.

[51] C. Gimbert-Suriñach, J. Albero, T. Stoll, J. Fortage, M.N. Collomb, A. Deronzier, E. Palomares, A. Llobet, Efficient and limiting reactions in aqueous light-induced hydrogen evolution systems using molecular catalysts and quantum dots, J. Am. Chem. Soc. 136 (2014) 7655–7661, https://doi.org/10.1021/ja501489h.

[52] H. Song, Y. Li, L. Shang, Z. Tang, T. Zhang, S. Lu, Designed controllable nitrogen-doped carbon-dots-loaded MoP nanoparticles for boosting hydrogen evolution reaction in alkaline medium, Nano Energy 72 (2020) 104730, https://doi.org/10.1016/j.nanoen.2020.104730.

[53] A. Alobaid, C. Wang, R.A. Adomaitis, Mechanism and kinetics of HER and OER on NiFe LDH films in an alkaline electrolyte, J. Electrochem. Soc. 165 (2018) J3395–J3404, https://doi.org/10.1149/2.0481815jes.

[54] Y. Zhou, S. Yang, D. Fan, J. Reilly, H. Zhang, W. Yao, J. Huang, Carbon quantum dot/TiO2 nanohybrids: efficient photocatalysts for hydrogen generation via intimate contact and efficient charge separation, ACS Appl. Nano Mater. 2 (2019) 1027–1032, https://doi.org/10.1021/acsanm.8b02310.

[55] N.Y. Donkadokula, A.K. Kola, I. Naz, D. Saroj, A review on advanced physico-chemical and biological textile dye wastewater treatment techniques, Rev. Environ. Sci. Biotechnol. 19 (2020) 543–560, https://doi.org/10.1007/s11157-020-09543-z.

[56] F. Lu, D. Astruc, Nanocatalysts and other nanomaterials for water remediation from organic pollutants, Coord. Chem. Rev. 408 (2020) 213180, https://doi.org/10.1016/j.ccr.2020.213180.

[57] Y. Areerob, J.Y. Cho, W.K. Jang, W.C. Oh, Enhanced sonocatalytic degradation of organic dyes from aqueous solutions by novel synthesis of mesoporous Fe3O4-graphene/ZnO@SiO2 nanocomposites, Ultrason. Sonochem. 41 (2018) 267–278, https://doi.org/10.1016/j.ultsonch.2017.09.034.

[58] S. Farhadi, F. Siadatnasab, Sonocatalytic degradation of organic pollutants by CdS nanoparticles hydrothermally prepared from cadmium(II) diethanoldithiocarbamate, Desalination Water Treat. 66 (2017) 299–308, https://doi.org/10.5004/dwt.2016.0096.

[59] M. Ahmad, E. Ahmed, Z.L. Hong, W. Ahmed, A. Elhissi, N.R. Khalid, Photocatalytic, sonocatalytic and sonophotocatalytic degradation of Rhodamine B using ZnO/CNTs composites photocatalysts, Ultrason. Sonochem. 21 (2014) 761–773, https://doi.org/10.1016/j.ultsonch.2013.08.014.

[60] L. Song, Y. Li, S. Zhang, Sonocatalytic degradation of rhodamine B in presence of CdS, Environ. Sci. Pollut. Control Ser. 25 (2018) 10714–10719, https://doi.org/10.1007/s11356-018-1369-8.

[61] Z. Da Meng, L. Zhu, J.G. Choi, C.Y. Park, W.C. Oh, Sonocatalytic degradation of Rhodamine B in the presence of C60 and CdS coupled TiO2 particles, Ultrason. Sonochem. 19 (2012) 143–150, https://doi.org/10.1016/j.ultsonch.2011.05.006.
[62] C. Lops, A. Ancona, K. Di Cesare, B. Dumontel, N. Garino, G. Canavese, S. Hérnandez, V. Cauda, Sonophotocatalytic degradation mechanisms of Rhodamine B dye via radicals generation by micro- and nano-particles of ZnO, Appl. Catal. B Environ. 243 (2019) 629–640, https://doi.org/10.1016/j.apcatb.2018.10.078.
[63] I. Fatimah, R. Nurillahi, I. Sahroni, G. Fadillah, B.H. Nugroho, A. Kamari, O. Muraza, Sonocatalytic degradation of rhodamine B using tin oxide/montmorillonite, J. Water Proc. Eng. 37 (2020) 101418, https://doi.org/10.1016/j.jwpe.2020.101418.
[64] K. Okitsu, B. Nanzai, K. Kawasaki, N. Takenaka, H. Bandow, Sonochemical decomposition of organic acids in aqueous solution: understanding of molecular behavior during cavitation by the analysis of a heterogeneous reaction kinetics model, Ultrason. Sonochem. 16 (2009) 155–162, https://doi.org/10.1016/j.ultsonch.2008.06.006.
[65] A. Selim, S. Kaur, A.H. Dar, S. Sartaliya, G. Jayamurugan, Synergistic effects of carbon dots and palladium nanoparticles enhance the sonocatalytic performance for rhodamine B degradation in the absence of light, ACS Omega 5 (2020) 22603–22613, https://doi.org/10.1021/acsomega.0c03312.